Journal of Applied Physics

Fabrication and characterization of nanostructured Fe_3S_4, an isostructural compound of half-metallic Fe_3O_4

Cite as: J. Appl. Phys. **117**, 223903 (2015); https://doi.org/10.1063/1.4922578
Submitted: 05 May 2015 . Accepted: 03 June 2015 . Published Online: 10 June 2015

Peng Li, Chuan Xia, Qiang Zhang, Zaibing Guo, Wenyao Cui, Haili Bai, Husam N. Alshareef, and Xi-xiang Zhang

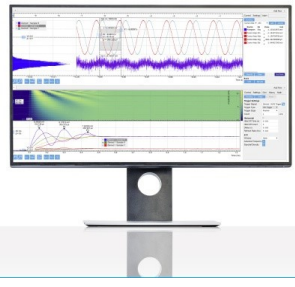

Fabrication and characterization of nanostructured Fe_3S_4, an isostructural compound of half-metallic Fe_3O_4

Peng Li,[1,2] Chuan Xia,[1] Qiang Zhang,[1] Zaibing Guo,[3] Wenyao Cui,[2] Haili Bai,[2] Husam N. Alshareef,[1] and Xi-xiang Zhang[1,a)]

[1]*Division of Physical Science and Engineering, King Abdullah University of Science and Technology (KAUST), Thuwal 23955, Kingdom of Saudi Arabia*

[2]*Tianjin Key Laboratory of Low Dimensional Materials Physics and Preparing Technology, Faculty of Science, Institute of Advanced Materials Physics, Tianjin University, Tianjin 300072, People's Republic of China*

[3]*Advanced Nanofabrication, Imaging and Characterization Core Lab, King Abdullah University of Science and Technology, Thuwal-239955, Kingdom of Saudi Arabia*

(Received 5 May 2015; accepted 3 June 2015; published online 10 June 2015)

High-purity, well-crystallized spinel Fe_3S_4 nanoplatelets were synthesized by the hydrothermal method, and the saturation magnetic moment of Fe_3S_4 was measured at 1.83 μ_B/f.u. The temperature-dependent resistivity of Fe_3S_4 was metallic-like for $T < 180$ K: room-temperature resistivity was measured at 7.711×10^3 $\mu\Omega$ cm. The anomalous Hall conductivity of Fe_3S_4 decreased with increasing longitudinal conductivity, in sharp contrast with the accepted theory of the anomalous Hall effect in a dirty-metal regime. Furthermore, negligible spin-dependent magnetoresistance was observed. Band structure calculations confirmed our experimental observations that Fe_3S_4 is a metal and not a half metal as expected. © *2015 AIP Publishing LLC*. [http://dx.doi.org/10.1063/1.4922578]

INTRODUCTION

Half a century ago, Skinner first identified greigite (Fe_3S_4) in Californian sediments.[1] It is one of many iron sulfides and has an inverse spinel crystal structure that is isostructural to the iron oxide spinel Fe_3O_4 (magnetite) phase. Here, we experimentally explore the prediction made from first principle calculations that, like magnetite,[2–4] greigite is a half metal.[5–7] Because Fe_3S_4 has low metastability, few studies have successfully investigated its characteristics. For example, Fe_3S_4 is unstable at high temperatures even in an argon atmosphere[2] and easily converts to Fe_7S_8 at temperatures over 240 °C;[8] the crystal structures of most iron sulfides $Fe_{1-x}S$ are rather complicated. In addition to interests in its electric properties, greigite has also attracted considerable attention for its potential application in high-energy storage based on reversible redox reactions in alkaline electrolytes, and to catalytic and biomedical fields.[9–12]

Ascribed to the larger ion radius of sulfur than oxygen, the lattice constant of Fe_3S_4 (9.876 Å) is larger than that of Fe_3O_4 (8.397 Å). Similar to Fe_3O_4, the magnetic configuration of Fe_3S_4 is expected to be ferrimagnetic ($(Fe^{3+})_A(Fe^{2+}Fe^{3+})_BS_4$),[13,14] with the iron spin moments on tetrahedral (A) sites antiparallel to the ones on octahedral (B) sites. The exchange coupling constant J_{AB} between A and B sites in Fe_3S_4 is approximately 1.03 meV lower than the 2.88 meV found in Fe_3O_4.[5] Consequently, the Néel temperature of Fe_3S_4 ($T_N = 667$ K) is lower than for Fe_3O_4 ($T_N = 858$ K).[6] Compared with the extensively studied half-metallic Fe_3O_4 and insulating ferrimagnetic spin filter $Ni(Co)Fe_2O_4$, few reports have investigated electrical or other physical properties of Fe_3S_4 because of the difficulty in obtaining high-purity thiospinel samples. To date, although several theoretical calculations predict a half-metallic band structure for Fe_3S_4, supporting experimental results are necessary to confirm this prediction.[5] For example, de Groot *et al*. claimed that Fe_3S_4 is, in fact, a normal metal with a switchable Fermi level.[15] For these reasons, we performed experimental investigations to determine the basic electrical and magnetotransport properties of Fe_3S_4.

In this work, high-purity, nanostructured Fe_3S_4 material was synthesized using the hydrothermal method. We observed negligible spin-dependent magnetoresistance in Fe_3S_4 between 2 K and 300 K. Band structure calculations indicate that Fe_3S_4 is a normal metal rather than a half-metal.

EXPERIMENTAL SECTION

We used the hydrothermal method to synthesize high-purity Fe_3S_4. First, nitrogen gas was bubbled for at least 30 min through deionized water (DI) to remove all dissolved oxygen before synthesis. Next, 1 mmol L-cysteine (C_3H_7NS, 0.121 g) was dissolved in 40 ml of DI water and $FeSO_4$ (1 mmol, 0.278 g) was added under constant and vigorous stirring. After thorough mixing, the mixture was transferred into a Teflon-sealed autoclave and heated to 200 °C for 20 h followed by natural cooling to room temperature. The resulting black precipitate was separated by centrifugation, rinsed with ethanol and dried at room temperature.

The structure was analyzed by x-ray diffraction (XRD), Raman spectra, scanning electron microscope (SEM), and transmittance electron microscope (TEM) images. We measured the magnetic properties using a Quantum Design magnetic property measurement system. The Fe_3S_4 powder was

a)Author to whom all correspondence should be addressed. Electronic mail: xixiang.zhang@kaust.edu.sa

hydraulically cold pressed at 774 MPa into $3 \times 10 \times 0.5$ mm pellets to measure the transport properties; magnetotransport properties were measured with a physical property measurement system (PPMS-9, Quantum Design).

Calculations made within the density function theory were performed using the Vienna *ab initio* simulation package code[16,17] The inner electrons consisting of orbitals up to, and including, the 3p levels for Fe, the 2 p level for S, and the 1 s for O were described by the projector augmented wave (PAW) method.[18] Calculations were carried out on a spinel cubic cell containing 56 atoms (24 Fe and 32 S) in the reciprocal space of the cell and were computed with a Monkhorst-Pack grid of $4 \times 4 \times 4$ k points.[19] The optimized parameters of the 56-atom, highly symmetrical unit cell were measured at Hubbard correction $U_{\text{eff}} = 0.7$, 1.0, 1.3, 1.5, 2.5, and 3.8 eV by modifying the same orbitals as in Fe_3S_4. To demonstrate the validity of this method, we calculated the band structures of Fe_3O_4 with $U_{\text{eff}} = 3.6$ eV as a comparison.

RESULTS AND DISCUSSION

Figure 1(a) shows the XRD patterns we obtained from our samples. All diffraction peaks were indexed to a standard Fe_3S_4 spinel structure with no detectable second phase. Furthermore, the relative intensity among the diffraction peaks was consistent with the standard spinel structure, indicative of the successful and controlled synthesis of metastable thiospinel Fe_3S_4 using the hydrothermal method. We calculated the lattice constant of Fe_3S_4 to be 9.811 Å. Next, we performed Raman scattering experiments in air and in argon to confirm the crystal structure of Fe_3S_4, as shown in Figure 1(b). All vibration modes obtained in the argon environment could be assigned to Fe_3S_4, confirming the high purity and good crystallinity of the sample, while those obtained in air could be assigned to Fe_3O_4, indicative of the oxidation of Fe_3S_4 by laser heating in air.

With the quality of the sample confirmed, we used SEM to investigate the morphology of the Fe_3S_4 crystallites. Figures 1(c) and 1(d) illustrate the formation of Fe_3S_4 microflowers, each consisting of a number of nanoplatelets 5–8 μm in width and length and 0.5 μm in thickness. The gaps between these larger micron-sized platelets are filled with much smaller platelets, consistent with observations by Cao *et al.*[20,21] We performed energy-dispersive X-ray spectroscopy (EDX) and element mapping to learn more about the elemental composition and distribution in these microflowers (Figure 1(d)). The signal of aluminum is from the sample holder. The atomic ratio of iron to sulfur was calculated at 0.752, similar to the ratio for stoichiometric Fe_3S_4. It is evident that the Fe (K) and S (K) elemental mapping is in good agreement with the morphology in Figure 1(d). The stoichiometric composition and the uniform distribution of elements is also evidence for the high quality of our materials. Figure 1(e) presents the images of an ultrathin nanoplatelet and the corresponding selected area electron diffraction. Although most of the diffraction spots were strong and hexagonal (red circles),[22] a few were relatively weak (green circles), and all could be assigned to the Fe_3S_4 lattice planes. The superposition of diffraction patterns of different axes

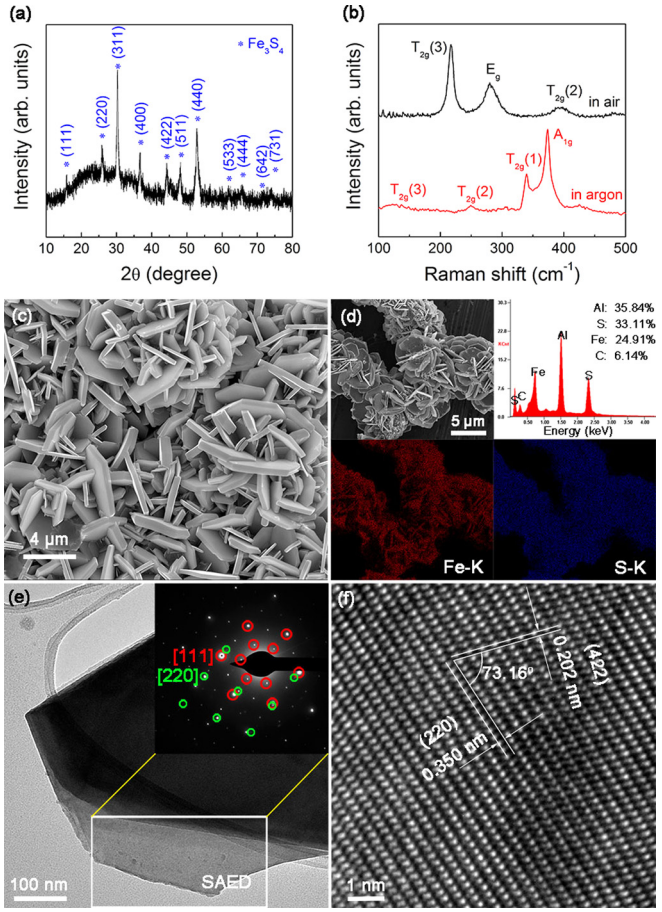

FIG. 1. (a) A typical XRD pattern of Fe_3S_4 with all the diffraction peaks typical of spinel Fe_3S_4. (b) The Raman spectrum of Fe_3S_4 in air and in argon atmospheres. (c) Typical morphology of Fe_3S_4. (d) EDX analysis and element mapping for elemental Fe and S. (e) A TEM image for Fe_3S_4 nanoplatelet obtained by ultrasonic process; the inset shows the selected area electron diffraction patterns of the edge of the nanoplatelet. Two sets of diffraction spot patterns are evident: Red represents [111] and green represents [220]. (f) A high-resolution TEM image for the Fe_3S_4 nanoplatelet. The labeled lattice plane ((422) and (220)) distance and angle are consistent with the spinel structure of Fe_3S_4.

further confirmed the good crystallinity and polycrystalline nature of the layered Fe_3S_4 nanoplatelets. The high-resolution TEM image shown in Figure 1(f) exhibits two sets of lattice planes (422) and (220) based on lattice plane distances 0.202 and 0.350 nm, respectively, which agree with the lattice constant of Fe_3S_4 (9.811 Å). The angle between (422) and (220) is 73.16°, which is consistent with the expected value for the spinel with an anion face-centered cubic lattice cell.

Figure 2(a) shows the temperature-dependent magnetization of Fe_3S_4 measured by following zero-field-cooling and field-cooling processes under a 300 Oe magnetic field. Unlike the clear Verwey transition (~120 K) observed in Fe_3O_4,[2] we observed no magnetic phase transition in Fe_3S_4 throughout the temperature range. The magnetic hysteresis loops measured at different temperatures are shown in Figure 2(b). The saturation moment was measured at 1.83 μ_B/f.u. (34.53 emu/g) with a 50 kOe magnetic field, much smaller than the estimated moment of 4 μ_B/f.u. (75.45 emu/g) for the ideal ferrimagnetic configuration of inverse spinel Fe_3S_4. Our measured value is roughly consistent with that obtained by Coey *et al.*

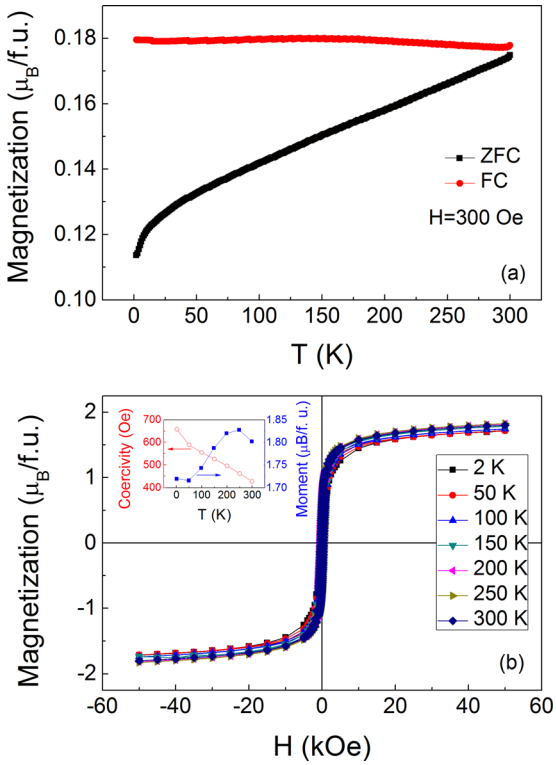

FIG. 2. (a) The temperature dependence of Fe_3S_4 zero-field-cooling and field-cooling magnetization at $H = 300$ Oe. (b) Hysteresis loops of Fe_3S_4 at different temperatures; the inset shows the coercivity variation.

(~2.0 μ_B/f.u.) but much smaller than that obtained by Li *et al* (~3.74 μ_B/f.u.).[13,14,23,24] The Curie temperature was much higher than room temperature, possibly as high as the reported $T_c = 677$ K.[6] The coercivity field decreased from 657 Oe at 2 K to 426 Oe at room temperature (~300 K) (the inset of Figure 2(b)). At this time, we are not able to explain the discrepancy between the experimental saturation magnetization and the theoretical values.[13,14] Based on the good crystallinity and high purity of the micron-sized grain of the materials, the measured saturation magnetization should reflect the intrinsic properties of single crystal-like bulk Fe_3S_4. Therefore, although their atomic structures are the same, it seems that Fe_3S_4 and Fe_3O_4 have different magnetic structures. The spin moment on A sites and B sites probably does not align as parallel nor antiparallel as Fe_3O_4, i.e., spin canting state.

To learn more about the electronic structures of Fe_3S_4, the temperature-dependence of resistivity was measured on a pellet, prepared by pressing Fe_3S_4 powder under a pressure of 774 MPa as shown in Figure 3(a). The room-temperature resistivity was found to be approximately 7.711×10^3 $\mu\Omega$ cm, which is consistent with previous studies;[25] however, the overall behavior of the temperature-dependent resistivity appears to be complex. For example, when the temperature was deceased from 300 K to 2 K, the resistivity first increased to a maximum near 180 K and then decreased to a minimum at 15 K; however, as the temperature continued to decrease to 2 K, the resistivity began to increase again. The broad maximum at around 180 K could be considered to be a metal-insulator-like transition, which was also observed by Guowei Li *et al.* at 100 K.[24] The origin of this metal-insulator transition is probably correlated with the breakdown of the Fe^{3+}/Fe^{2+} pair-charge order on octahedral sites, which is similar to the behavior of perovskite manganese oxides. Alternatively, negligible magnetoresistance was observed near the broad peak in Fe_3S_4 (Figure 3(b)), indicating that the electrical transport mechanism underlying this metal-insulator transition is different from that of perovskite manganese oxides, which have a large magnetoresistance that can be observed at the metal-insulator transition. This increase in resistivity with decreasing temperature for $T < 20$ K can be ascribed to the three-dimensional weak localization effect. As shown in the inset of Figure 3(a), a linear dependence of ΔR on $\sqrt{T}$ was observed that cannot be explained by the two-dimensional weak localization model ($\Delta R/R^2 \sim \ln T$).[26] Effects from this model are expected to present by electron scattering caused by the defects and

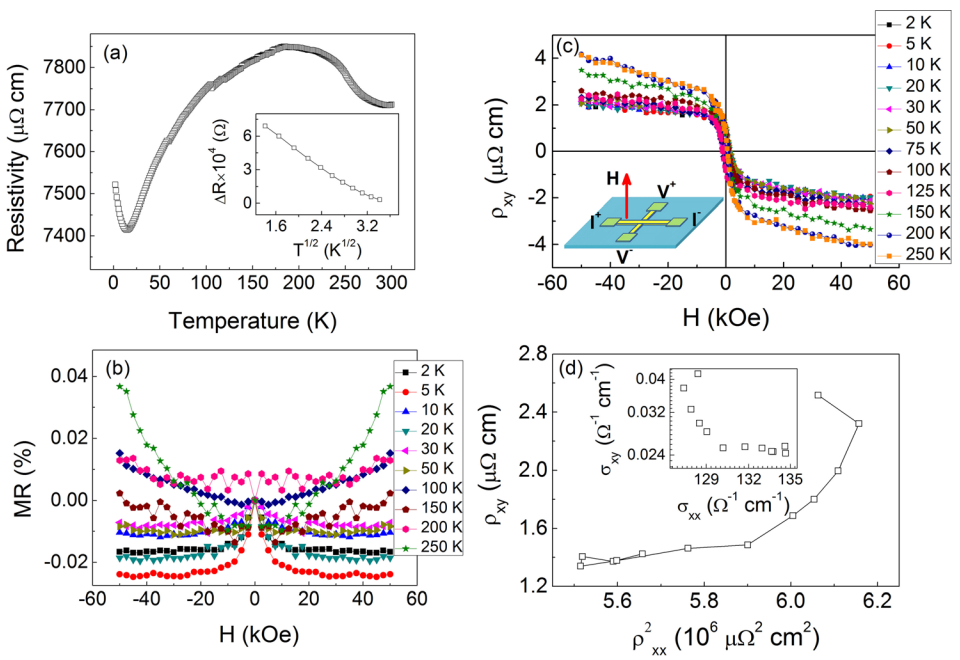

FIG. 3. (a) Temperature dependence of Fe_3S_4 resistivity; the inset gives the linear relation between ΔR and $\sqrt{T}$, indicative of three-dimensional weak localization at low temperatures. (b) The magnetoresistance of Fe_3S_4 at different temperatures. (c) Magnetic-field-dependent Hall resistivity of Fe_3S_4 at different temperatures; the inset gives the Hall measurement configuration. (d) The scaling relationship between anomalous Hall resistivity ρ_{xy}^{AHE} and resistivity ρ_{xx}; the inset shows the corresponding scaling relationship of conductivity.

interfaces between the crystal grains. Antiphase boundaries are commonly observed natural growth defects for cation sublattices in spinel materials, across from which forms the Fe-anion-Fe antiferromagnetic coupling due to a near 180° bond angle.[27] In fact, the weak saturation magnetization at high magnetic fields in Figure 2(b) is indicative of this type of superexchange interaction. It is well-known that the negative magnetoresistance commonly observed in polycrystalline, epitaxial Fe_3O_4 films and Fe_3O_4 particle systems is a result of spin-related scattering by antiphase boundaries or spin-related tunneling across grain boundaries caused by spin polarization in Fe_3O_4 (or a half-metallic characteristic of Fe_3O_4).[28–32] For this reason, if Fe_3S_4 is a half-metal or has spin-polarized electrical transport characteristics, it would be expected to have a sizable magnetoresistance. However, Figure 3(b) shows that negligible magnetoresistance was observed over the whole temperature range in comparison with the magnetoresistance observed for Fe_3O_4.[28–32] The minimal negative magnetoresistance observed at low temperatures ($T < 30$ K) can be attributed to a collapse in weak localization under the magnetic field.

The field dependence of Hall resistivity for pressed Fe_3S_4 pellet is presented in Figure 3(c). Because Hall resistances at different temperatures shifted slightly as a result of contributions from longitudinal resistivity (ρ_{xx}), all curves were corrected by removing contributions by longitudinal resistance. The bottom left inset in Figure 3(c) displays the schematic diagram for the Hall measurement configuration. Here, it is evident that the field-dependent Hall resistivity behaves differently at different temperatures. The curves obtained at temperatures below 125 K saturate to a lower anomalous Hall resistivity (1.8 $\mu\Omega$ cm) than values for curves obtained at higher temperatures ($T > 150$ K). More importantly, after magnetic saturation, the slope of curves at higher temperatures ($T > 150$ K) was also greater than that of the low temperature curves. These differences in anomalous Hall resistivity and slopes cannot be caused by magnetization because there is no evidence of anomaly in magnetization in this temperature range, as was evidenced by the hysteresis loops and temperature-independent magnetic saturation in Figure 2(b). The Hall resistivity anomaly observed in Figure 3(c) may have a similar mechanism as the metal-insulator transition observed in the temperature-dependent resistivity curve (Figure 3(a)). The positive slope of the Hall resistivity as a function of the magnetic field (after magnetic saturation) over the entire temperature range, as shown in Figure 3(c), indicates that electrical transport in Fe_3S_4 is dominated by *p*-type (hole) carriers. The carrier density can be obtained using the slope of the curves after the magnetic saturation we observed in Figure 3(c), whose origin could in fact be the ordinary Hall effect. The largest carrier density (obtained from the smallest ordinary Hall coefficient $R_0 = 1/pe$), measured at 2 K, was calculated to be 4.42×10^{21} /cm^3 (1.42×10^{-9} m^3/C) and the smallest carrier density, measured at 150 K, was calculated to be 1.97×10^{21} /cm^3 (3.16×10^{-9} m^3/C) (see Figure 3(c)).

To better understand the nature of electrical transport and to better define the magnetic structures, we investigated the scaling of anomalous Hall resistivity with longitudinal resistivity, where the anomalous Hall resistivity ρ_{xy}^{AHE} was obtained by extrapolating the high-field portion of the curves in Figure 3(c) to $H = 0$. The Hall transport mechanism shown in Figure 3(d) cannot be explained by either side jump or intrinsic anomalous Hall effects, which predict a $\rho_{xy}^{AHE} \propto \rho_{xx}^2$ relationship.[33] It appears that Fe_3S_4 belongs to the bad-metal regime ($\sigma_{xx} < 10^4(\Omega\text{cm})^{-1}$). According to the unified theory, Hall conductivity conforms to the scaling law $\sigma_{xy} \propto \sigma_{xx}^n$ with $1.6 < n < 1.7$.[33] As presented in the inset of Figure 3(d), Hall conductivity σ_{xy} decreases with increasing conductivity σ_{xx}. This scaling relationship is completely different from the unified theory prediction, and more work is needed to provide a detailed explanation. For example, it would be interesting to vary the film thickness of Fe_3S_4 in an attempt to modulate anomalous Hall conductivity on a large scale.

Because we observed negligible effects from magnetoresistance in Fe_3S_4, we became curious about its band structure. After geometry optimization, the calculated thiospinel lattice parameters were 9.802, 9.860, 9.897, 9.924, 10.037, and 10.116 Å for the different Hubbard correction parameters $U_{eff} = 0.7$, 1.0, 1.3, 1.5, 2.5, and 3.8 eV, respectively. More detailed structural information (e.g., bond length and bond angle) is presented in Table I. Results show that, regardless of how large the U_{eff} value is, all bond angles (Fe(A)-anion-Fe(A), Fe(B)-anion-Fe(B), and Fe(A)- anion-Fe(B)) in Fe_3S_4 are similar to those in Fe_3O_4; however, as expected, because of the larger lattice constant and larger ionic radius, all bond lengths in Fe_3S_4 are longer than those in Fe_3O_4. Compared to Fe_3O_4 ($U_{eff} = 3.6$ eV), an electron correlation $U_{eff} = 0.7$ eV correction is closer to our experimental results (9.811 Å), in good agreement with Devey *et al.*[5] A detailed explanation describing Fe_3S_4 with $U_{eff} = 0.7$ eV will be discussed hereafter.

TABLE I. Comparison of structural parameters for Fe_3S_4 and Fe_3O_4.

Parameters	Fe_3S_4						Fe_3O_4
	$U = 0.7$	$U = 1.0$	$U = 1.3$	$U = 1.5$	$U = 2.5$	$U = 3.8$	$U = 3.6$
Lattice constant (Å)	9.802	9.860	9.897	9.924	10.037	10.116	8.487
d (FeA-S/O) (Å)	2.20603	2.20903	2.22026	2.22768	2.25839	2.28198	1.90859
d (FeB-S/O) (Å)	2.41591	2.42291	2.43063	2.43634	2.46113	2.47704	2.08161
FeA-S/O-FeA (deg)	116.44	116.42	116.39	116.38	116.34	116.29	116.35
FeA-S/O-FeB (deg)	123.83	123.83	123.78	123.75	123.64	123.53	123.67
FeB-S/O-FeB (deg)	91.94	92.01	92.08	92.12	92.27	92.43	92.23
$_m$ (μ_B/f.u.)	2.547	2.783	2.955	3.064	3.434	3.729	4.135

Figure 4 gives the total and partial density of states for Fe_3S_4 with different U_{eff}. For $U_{eff} = 3.8$ eV, similar to Fe_3O_4, only three spin-down t_{2g} electrons on B sites (xy, yz and zx) were present at the Fermi level in Fe_3S_4, with a relatively small energy gap of ~ 0.4 eV for spin-up electrons near the Fermi level. This indicates half metallicity of Fe_3S_4 with $U_{eff} = 3.8$ eV; however, the lattice constant 10.116 Å for $U_{eff} = 3.8$ eV is too large in comparison with the experimental value (9.811 Å). As U_{eff} decreases, the S p states are more inclined to hybridize Fe 3d (FeA 3d and FeB 3d) states from −5.5 to 3.5 eV. Given the stronger covalent nature of the Fe-S bond than that of the ionic Fe-O bond, a small U_{eff} correction ($U_{eff} = 0.7$ eV) is better suited to describe Fe_3S_4. As shown in Figure 4(a), the small energy gap for spin-up electrons disappears with decreasing U_{eff} (0.7 eV), which strongly suggests that Fe_3S_4 is a normal metal rather than a spin-polarized half metal. This result is consistent with calculations by de Groot *et al.*[15]

On the other hand, the strong hybridization between S p and Fe 3 d states caused by distinct spin splitting for Fe 3 d states (both A and B sites) becomes weaker with decreasing U_{eff}, resulting in a decrease in the spin moment from 3.729 μ_B/f.u. ($U_{eff} = 3.8$ eV) to 2.547 μ_B/f.u. ($U_{eff} = 0.7$ eV). It appears that the calculated spin moment (2.547 μ_B/f.u.) with $U_{eff} = 0.7$ eV is much closer to our measured moment for Fe_3S_4 (1.83 μ_B/f.u.). Compared to the ionic Fe-O bond in Fe_3O_4 ($T_C \sim 858$ K), the superexchange Fe(A)-anion(S)-Fe(B) in thiospinel Fe_3S_4 is mildly suppressed, inducing the decreased Curie temperature ($T_C \sim 677$ K).[6] Figure 5 shows a comparison of the charge density difference for Fe_3S_4 ($U_{eff} = 0.7$ eV) and Fe_3O_4 ($U_{eff} = 3.6$ eV), where the superexchange in Fe(A)-S-Fe(A), Fe(B)-S-Fe(B), and Fe(A)-S-Fe(B) was reduced considerably compared to that in Fe_3O_4.

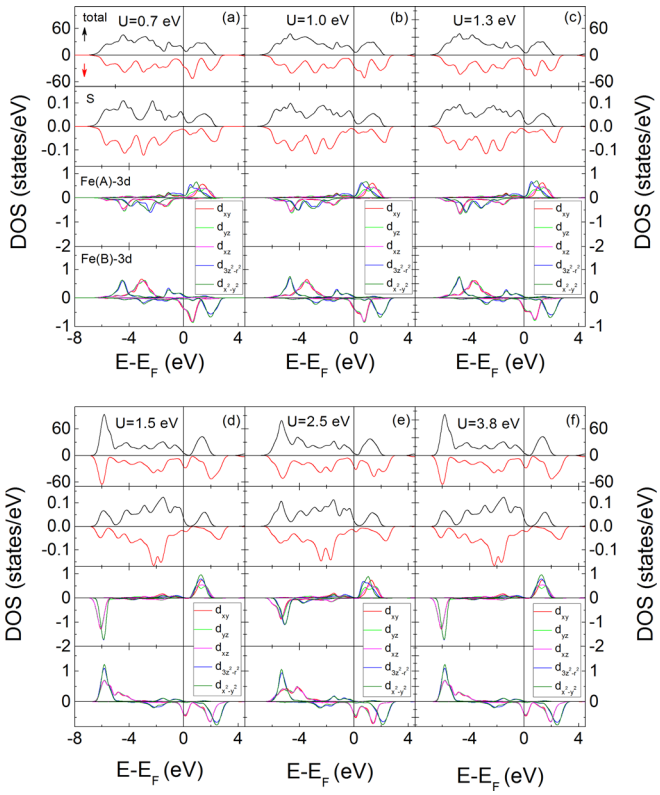

FIG. 4. Total and partial density of states (sulfur and iron on A and B sites) for Fe_3S_4 with different Hubbard correction parameters (a) $U_{eff} = 0.7$ eV, (b) $U_{eff} = 1.0$ eV, (c) $U_{eff} = 1.3$ eV, (d) $U_{eff} = 1.5$ eV, (e) $U_{eff} = 2.5$ eV, and (f) $U_{eff} = 3.8$ eV.

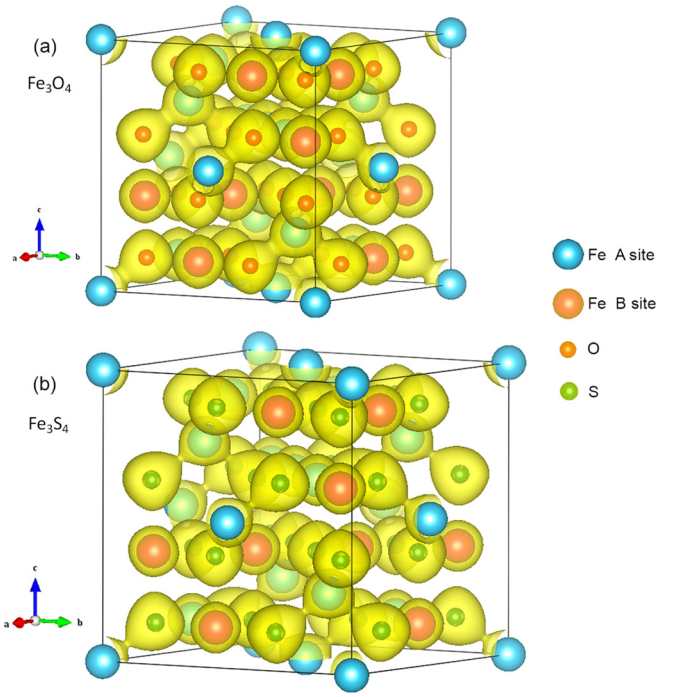

FIG. 5. Comparison of the charge density difference for Fe_3O_4 ($U_{eff} = 3.6$ eV) (a) and Fe_3S_4 ($U_{eff} = 0.7$ eV) (b).

CONCLUSIONS

In summary, we used the hydrothermal method to synthesize high-purity and stoichiometric spinel Fe_3S_4 samples. The saturation magnetic moment was found to be 1.83 μ_B/f.u. (34.53 emu/g) at room temperature and no magnetic phase transition was observed over a temperature range of 2 K to 300 K. We observed metallic-like transport behavior at $T < 180$ K. The anomalous Hall conductivity in Fe_3S_4 decreased with increasing longitudinal conductivity and could not be explained by the unified theory of the bad-metal regime. No spin-dependent magnetoresistance was observed in Fe_3S_4, which indicates that Fe_3S_4 is a normal metal rather than a half metal. Furthermore, theoretical calculations confirmed that Fe_3S_4 is a normal metal at the Fermi level. We suggest that the combination of the strong covalent character of Fe-S bonds and the hybridization between S p states and Fe 3 d states render Fe_3S_4 a normal metal rather than a half metal.

ACKNOWLEDGMENTS

This work was supported by a SABIC Postdoctoral Fellowship Award presented to King Abdullah University of Science and Technology (KAUST) in the Kingdom of Saudi Arabia, the National Science Foundation of China (Grant No. 11204207) and the Ph.D. Programs Foundation of the Ministry of Education of China (Grant

No. 20120032120074). Thanks to Yang Yang in core labs for performing the Raman measurement and analyses.

[1]B. J. Skinner, F. S. Grimaldi, and R. C. Erd, Am. Mineral **49**, 543 (1964).
[2]G. Q. Gong, A. Gupta, G. Xiao, W. Qian, and V. P. Dravid, Phys. Rev. B **56**, 5096 (1997).
[3]Y. S. Dedkov, U. Rudiger, and G. Guntherodt, Phys. Rev. B **65**, 064417 (2002).
[4]M. I. Katsnelson, V. Y. Irkhin, L. Chioncel, A. I. Lichtenstein, and R. A. de Groot, Rev. Mod. Phys. **80**, 315 (2008).
[5]A. J. Devey, R. Grau-Crespo, and N. H. de Leeuw, Phys. Rev. B **79**, 195126 (2009).
[6]J. Wang, S. H. Cao, W. Wu, and G. M. Zhao, Phys. Scr. **83**, 045702 (2011).
[7]A. Roldan, D. Santos-Carballal, and N. H. de Leeuw, J. Chem. Phys. **138**, 204712 (2013).
[8]H. F. Liu, A. Huang, and D. Z. Chi, J. Phys. D: Appl. Phys. **43**, 455405 (2010).
[9]C. T. Lefevre, N. Menguy, F. Abreu, U. Lins, M. Posfai, T. Prozorov, D. Pignol, R. B. Frankel, and D. A. Bazylinski, Science **334**, 1720 (2011).
[10]X. L. Jia, Z. Chen, X. Cui, Y. T. Peng, X. L. Wang, G. Wang, F. Wei, and Y. F. Lu, Acs Nano **6**, 9911 (2012).
[11]M. Naresh, S. Das, P. Mishra, and A. Mittal, Biotechnol. Bioeng. **109**, 1205 (2012).
[12]W. Chen, C. Xia, and H. N. Alshareef, Acs Nano **8**, 9531 (2014).
[13]J. M. D. Coey and M. R. Spender, Bull. Am. Phys. Soc. **15**, 824 (1970).
[14]J. M. D. Coey, M. R. Spender, and A. H. Morrish, Solid State Commun. **8**, 1605 (1970).
[15]B. Zhang, G. A. de Wijs, and R. A. de Groot, Phys. Rev. B **86**, 020406R (2012).
[16]G. Kresse and J. Hafner, Phys. Rev. B **47**, 558 (1993).
[17]G. Kresse and J. Furthmuller, Comput. Mater. Sci. **6**, 15 (1996).
[18]P. E. Blochl, Phys. Rev. B **50**, 17953 (1994).
[19]H. J. Monkhorst and J. D. Pack, Phys. Rev. B **13**, 5188 (1976).
[20]Z. B. He, Y. Shu-Hong, X. Y. Zhou, X. G. Li, and J. F. Qu, Adv. Funct. Mater. **16**, 1105 (2006).
[21]F. Cao, W. Hu, L. Zhou, W. D. Shi, S. Y. Song, Y. Q. Lei, S. Wang, and H. J. Zhang, Dalton Trans. **2009**, 9246.
[22]F. C. Meldrum, S. Mann, B. R. Heywood, R. B. Frankel, and D. A. Bazylinski, P. R. Soc. London, Ser. B **251**, 231 (1993).
[23]M. R. Spender, J. M. D. Coey, and A. H. Morrish, Can. J. Phys. **50**, 2313 (1972).
[24]G. W. Li, B. M. Zhang, F. Yu, A. A. Novakova, M. S. Krivenkov, T. Y. Kiseleva, L. Chang, J. C. Rao, A. O. Polyakov, G. R. Blake, R. A. de Groot, and T. T. M. Palstra, Chem. Mater. **26**, 5821 (2014).
[25]H. Nozaki, J. Appl. Phys. **51**, 486 (1980).
[26]Z. Q. Li and J. J. Lin, J. Appl. Phys. **96**, 5918 (2004).
[27]D. T. Margulies, F. T. Parker, M. L. Rudee, F. E. Spada, J. N. Chapman, P. R. Aitchison, and A. E. Berkowitz, Phys. Rev. Lett. **79**, 5162 (1997).
[28]J. M. D. Coey, A. E. Berkowitz, L. Balcells, F. F. Putris, and F. T. Parker, Appl. Phys. Lett. **72**, 734 (1998).
[29]M. Ziese and H. J. Blythe, J. Phys.-Condens. Matter **12**, 13 (2000).
[30]W. Eerenstein, T. T. M. Palstra, S. S. Saxena, and T. Hibma, Phys. Rev. Lett. **88**, 247204 (2002).
[31]H. Liu, E. Y. Jiang, H. L. Bai, R. K. Zheng, H. L. Wei, and X. X. Zhang, Appl. Phys. Lett. **83**, 3531 (2003).
[32]A. V. Ramos, J. B. Moussy, M. J. Guittet, A. M. Bataille, M. Gautier-Soyer, M. Viret, C. Gatel, P. Bayle-Guillemaud, and E. Snoeck, J. Appl. Phys. **100**, 103902 (2006).
[33]N. Nagaosa, J. Sinova, S. Onoda, A. H. MacDonald, and N. P. Ong, Rev. Mod. Phys. **82**, 1539 (2010).